International Journal of Engineering

Journal Homepage: www.ije.ir

Design of a High Range, High Efficiency Spread Spectrum Transmitter for Audio Communication Applications

S. Seifi*, H. Miar Naimi, S. M. H. Andargoli

Department of Electrical Engineering, Babol University of Technology, Babol, Iran

PAPER INFO

Paper history:
Received 05 November 2018
Received in revised form 23 April 2019
Accepted 02 May 2019

Keywords:
Direct Sequence Spread Spectrum
Double Balanced Passive Mixer
Error Vector Magnitude
Inverse E Power Amplifier
Switching Power Amplifier
Tunable Quadrature Oscillator
Wireless Transmitter

ABSTRACT

This work proposes a direct sequence spread spectrum transmitter with high transmission range and efficiency for audio signals. It is shown that by choosing high process gain for spread spectrum signal the data could reach a range of 55km in the 2.4GHz ISM band. By employing a light modulation scheme, we have a relaxed SNR requirement for having a low bit error rate (BER) which translates to relaxed error vector magnitude (EVM) condition. Therefore a switching power amplfier (PA) is used in this work which improves the transmitter's efficiency while by taking PAs nonidealities into account we extracted the new equations to find the conditions to improve the efficiency compared to conventional zero current and zero current switching conditions. The PA efficiency is equal to 79.5% while having 30dBm output power. The mixer alongside power amplifier used in this work provide a conversion gain of 9 dB while having 16 dBm output compression point. The employed tunable quadrature oscillator has the ability to cancel phase and amplitude errors without comprimising the oscillator phase noise. The transmitter reaches an efficiency of 73.4% and an EVM of -32.75 dB.

***doi**: 10.5829/ije.2019.32.08b.10*

1. INTRODUCTION

Wireless communications as a fast growing and widely spread technology with higher flexibility and lower cost compared to wired communications is an inseparable part of the modern life [1–3]. Among various methods of multiple access, direct sequence spread spectrum (DSSS) systems gain popularity nowadays. Because of using pseudorandom codes to spread the baseband data, communication is very hard to intercept [4], and also low power density imposes very little noise to near communication bands. The use of orthogonal spreading code also makes the system tolerant in facing jammers [5]. The usual architectures for a transmitter design are direct conversion, modern direct conversion and heterodyne architectures.

The heterodyne architecture performs the signal upconversion in two steps so that the LO frequency remains far from the PA output spectrum [6]. Because the I/Q upconversion occurs at a significantly lower frequeney than the carrier, it exhibits smaller gain and phase mismatches. Also the upconverter frequencies are quite far from the signal output spectrum, therefore the injection pulling is not an issue here but on the other hand the mixing spurs caused from the two upconverters would pollute the output spectrum. Because of the image problem, a baseband filter is also needed which alongside the two upconverters would increase the cost and needed chip area [6].

Direct conversion transmitters on the other hand directly translate the baseband spectrum to the RF carrier frequency. In this architecture, the upconverter is followed by a PA and a matching network whose role is to provide maximum power delivery to the antenna and filter out-of-band components that result from the PA nonlinearity [6]. The simplicity, low power consumption and needed chip area makes direct conversion transmitters gain attention among RF designers [7, 8].

Because of the direct translation to the RF frequency there are no mixing spurs in the output spectrum but the quadrature mismatches which are a result of the mixer

*Corresponding Author Email: *s.seifi65@yahoo.com* (S. Seifi)

Please cite this article as: S. Seifi, H. Miar Naimi, S. M. H. Andargoli, Design of a High Range, High Efficiency Spread Spectrum Transmitter for Audio Communication Applications, International Journal of Engineering (IJE), IJE TRANSACTIONS B: Applications Vol. 32, No. 8, (August 2019) 1144-1154

and oscillator mismatches [9, 10] are of importance because of high frequency implementation compared to heterodyne transmitter. The equality of upconverter and output spectrum center frequency makes LO pulling another issue to consider for the designers [11, 12]. Although the differential Power amplifier and symmetrical layout design can reduce the LO pulling significantly [6]. To overcome the LO pulling, modern direct conversion transmitters are proposed which choose the oscillator frequency far from the carrier frequency. The frequency division and mixing structure do so by choosing the LO frequency twice the frquency of carrier [13] which not only greatly reduces injection pulling but also readily provides quadrature phases for the carrier but because of the upconverter implementation at twice the operating frequency the divider speed could be the design bottleneck. Other approaches to reduce the LO pulling are the self mixing and single sideband mixing architectures [14, 15]. Self mixing basically uses a divide by two circuit and then mixes the LO with the dividers output to reach 3/2 times the LO frequency. This approach reduces the LO pulling but there is the image problem in 1/2 LO frequency which dissipates half the generated power and must be filtered that adds to the cost, complexity and the chip size. The single sideband architecture mixes two sufficiently far LO frequencies from the carrier to reduce the injection pulling. The two oscillators are implemented in the lower frequencies which reduces the parasitics effects but the need for two quadrature oscillators not only increases the cost and chip size but also introduces more mismatches to the output spectrum. In addition, the mixing spurs due to the two mixers would also pollute the output spectrum.

The mentioned architectures each have some advantages over others but because of its low cost, high efficiency and relative clean output spectrum, the direct conversion architecture is used in this work to implement the spread spectrum transmitter. Figure 1 shows the block diagram of the transmitter.

The rest of the paper is as follows. In section 2 the system design parameters are derived with focus to have the best possible range among the license free bands. Section 3, discusses the design of the power amplifier and shows that in presence of nonidealities the conventional conditions for efficiency is not true and then finds the best efficiency for the target output power. Proposing new conditions for improving PA efficiency (the most power hungry block of the transmiter) is the main contribution of this work which significantly improves the overall transmitter efficiency. Sections 4 and 5 focus on the upconverter alongside quadrature oscillator which is needed for frequency translation. Finally section 6 illustates the designed transmitter characteristics and section 7 discusses the conclusions of this work.

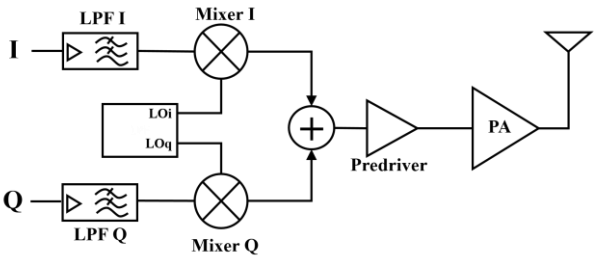

Figure 1. block diagram of the direct conversion transmitter

2. SYSTEM DESIGN

The equation to relate the transmission range to the receiver (Ps) and transmitter (Pr) power is defined as Equation (1) [16].

$$\frac{P_S}{\Pr(R)} = \left(\frac{4\pi fR}{c}\right)^2 \tag{1}$$

where, λ and C are the light wavelength and speed and 'f' denotes frequency. Note that the received power is a function of distance (R).

Considering an even power distibution in the signal bandwidth (B), the range of transimission can be found as Equation (2).

$$R = \frac{c}{(4\pi f_c)}\sqrt{\frac{P_S}{P_r}\left(\frac{1}{\left(1-\left(\frac{B}{2f_c}\right)^2\right)}\right)} \tag{2}$$

when $B<<2f_c$, Equation (2) can be simplified to Equation (3).

$$R = \frac{c}{(4\pi f_c)}\sqrt{\frac{P_S}{P_r}} \tag{3}$$

As it can be seen the range of transimission is inversely proportional to the frequency. So the frequency should be high enough to provide the needed bandwidth but not too high to limit the transmission range. Not to mention that implementing circuits in higher frequencies pose some challenges for the designer. Table 1 shows the ISM license free bands all around the world.

TABLE 1. The license free ISM bands worldwide

Spectrum number	1	2	3	4	5	6
Center frequency	13.56 MHz	27.12 MHz	40.68 MHz	2.44 GHz	5.8 GHz	24.125 GHz
Band width	14 KHz	326 KHz	40 KHz	80 MHz	150 MHz	250 MHz

The spectrum numbers 1, 2 and 3 could not provide enough bandwidth for a spread spectrum system and number 6 limits the transmission range because of the high center frequency. So the remaining spectrums are 2.4 and 5.8 GHz. The transmitted power limit for these two bands is 1 W.

According to (3), to increase the transmission range the received signal power density is considered 10 times lower than the noise. This will also prevent the signal to jam other receivers. Using this fact and (3) will give us 55 km transmission range for 2.44 GHz while 5.8 GHz band could only reach 16 km. Therefore, in terms of transmission range the 2.44 GHz band is a better choice.

On the other hand the low received power makes it hard to accurately detect the data. To further investigate this, receiver chain is depicted in Figure 2.

As it can be seen in Figure 2, the received signal ($P_r(R)$) is first amplified by LNA and then downconverted by the mixer to reach the processor ($P_d(R)$). $P_d(R)$ which is spread across B then is multiplied by the spreading code to translate the received signal to the narrowband version (BW). This will increase the signal SNR and facilitates the detectability process. The ratio of the spread (B) to narrowband signal (BW) bandwidth is called process gain and can be defined as Equation (4).

$$n = \frac{B}{BW} \tag{4}$$

It is obvious that greater process gain could improve the received signal's SNR to be more detectable by the receiver. The signal to noise ratio after processor (SNR_p) can be defined as Equation (5) [6].

$$SNR_p = SNR_R - \mathrm{NF} + 10\log n \tag{5}$$

where, SNR_R is the signal to noise ratio before recevier and NF is the receiver's noise figure.

To accurately detect the received signal, SNR_p should be higher than the minimum SNR needed to achieve the desired BER (bit error rate). BER is expressed by E_b/N_0 in which E_b is the bit energy and N_0 is the noise power density which also relates to M-PSK signal SNR by Equation (6).

$$SNR = \frac{E_b}{N_0} \times \log_2^M \tag{6}$$

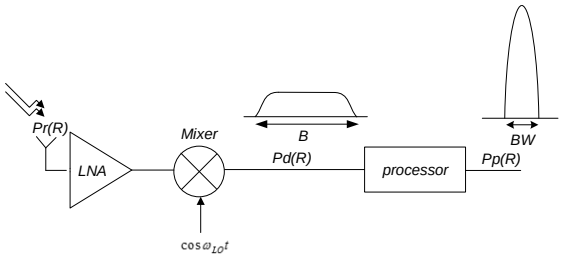

Figure 2. The receiver chain

Figure 3 shows the BER versus E_b/N_0 for different M-PSK modulation schemes [17].

By using Equation (6) and Figure 3 the minimum SNR needed to achieve BER=0.001 for different modulation schemes is extracted and shown in Table 2.

As it can be seen in Table 2, more dense modulations need higher SNR to detect the data which in turn limit the room for NF (Equation (5)) and make the receiver harder to implement. Another solution is to choose a higher process gain which leaves little room for unspread data. So lighter modulation schemes would be a better choice. On the other hand, since asymmetrical spectrums need to be demodulated using quadrature downconverters [6], the best choice for the modulation scheme is QPSK. Therefore Equation (5) can be rewritten for QPSK as Equation (7).

$$10\log n - \mathrm{NF} = 20 \tag{7}$$

The receiver NF should be low and the process gain should be high enough in order for Equation (7) to come true. For a 2048 spreading code length the process gain would be equal to 33dB which implies a 13dB room for receiver's NF that is quite reachable [6]. On the other hand 2048 bit spreading code leaves approximately

20KHz bandwidth for unspread data which can contain 40 kpbs raw data using QPSK modulation. This data rate is high enough to maintain an audio communication [18]. Table 3 shows the system design parameters of the transmiter.

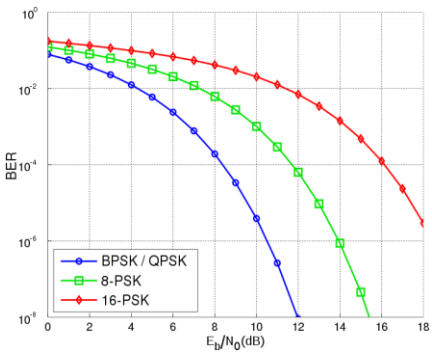

Figure 3. BER versus E_b/N_0 for different M-PSK modulation schemes

TABLE 2. Minimum SNR needed to achieve BER=0.001 for different modulation schemes

Spectrum number	BPSK	QPSK (4-PSK)	8-PSK	16-PSK
SNR_{min} (dB)	7	10	13	18

TABLE 3. System design parameters of the transmitter

Multiple aceess technique	Mod. scheme	Spreading code length	Center frequency	Comm. bandwidth	Raw data BW
DSSS	QPSK	2048	2.4GHz	80MHz	40 KHz

3. POWER AMPLIFIER DESIGN

Because of using light modulation scheme (QPSK) in this work there is no need for a linear power amplifier. Since power amplifier is the most power hungry block of the transmitter, utilizing nonlinear PAs will significantly improve the transmitter efficiency. Among different switching (nonlinear) PAs, class D uses two switches which could theoretically reach 100% efficiency but the timing issues of the two switches and the problem of driving an ungrounded switch in high frequency deviates the results from the ideal case [19]. Class E PAs utilize only one switch which does not have class D timing problems and by applying zero voltage and zero voltage derivative switching conditions could reach the theoretical efficiency of 100% considering ideal switch [20–22] but the main problem for class E power amplifier is the high peak switch voltage. In fact, [23] showed that the peak switch voltage is equal to $3.6V_{DD}$ which could reduce circuit reliability.

On the other hand class inverse E has 20% less peak switch voltage than class E and can achieve the theoritical 100% efficicency for ideal switch using zero current switching (ZCS) and zero current derivative switching (ZCDS) conditions [24, 25]. So, in this work we used inverse E power amplifier. Although the peak switch voltage is less than class E but it certainly passes $2V_{dd}$ and could cause circuit failure. So the stacked topology is used to relieve the voltage stress on the switch. Since PA nonlinearilties could increase the signal EVM which deteriorates BER, the PA is desinged to have a differential topology. Figure 4 shows the stacked differential inverse E power amplifier.

The circuit in the gray dashed area provides the bias needed for M2. While M3 reduces the voltage stress on M2. The DC block capacitor eliminates the output DC component while the Lp-Cp tank takes care of other harmonics except the fundemental one and the capacitor C provides the phase shift between input and output voltages. A balun is used to convert the differential signal to single ended to be suitable for the antenna.

The previous works for inverse E PAs consider an ideal switch so the optimal conditions for best efficiency would be ZCS and ZCDS but in reality the switch has finite resistance and capacitance associated with it which degrades the efficiency so the ZCS and ZCDS may not be the best choices. The effect of parasitic capacitance and resistance would be more noticeable when the switch is stacked to avoid voltage stress. So here we first find the equations needed for designing the PA considering arbitary values for current switch and its derivative in transistion from ON to OFF state (we call them i_0 and s_0 respectively) and extract efficiency versus these two parameters to show that ZCS and ZCDS conditions are not the best choices for efficiency in presence of switch nonidealities. Because of the differential nature of the circuit, the half circuit should provide 500 mW, and M2 and M3 can be modelled by a switch with C_{sw} and R_{sw} as equivalent switch output capacitance and resistance respectively. The simplified half circuit is shown in Figure 5.

Note that the duty cycle of input voltage is equal to 50% and the switch is ON for ($0<\theta<\pi$) and OFF for ($\pi<\theta<2\pi$) and the $L_{tank}C_{tank}$ resonator quality factor is high enough to consider V_{load} sinusoidal. So Equation (8) can be written for the output voltage [26].

$$V_{load} = V_{DD}.a.\sin(\theta+\varphi) \tag{8}$$

where, $V_{DD}.a$ is the output voltage amplitude which is a factor of the power supply V_{DD} and $\theta=\omega t$ where ω is the operating angular frequency, t denotes time and φ is the phase difference between input and output voltage.

The switch voltage can be written as Equation (9).

$$V_{sw},eq = \begin{cases} R_{sw,eq} i_{sw} & 0<\theta<\pi \\ V_{DD} - V_{load} & \pi<\theta<2\pi \end{cases} \tag{9}$$

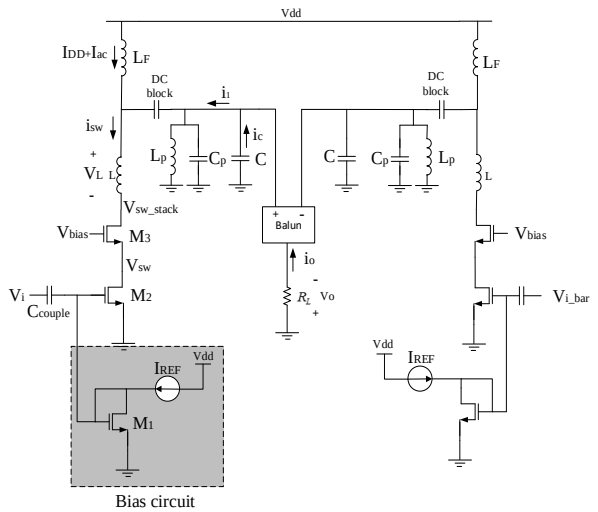

Figure 4. Stacked differential E inverse PA

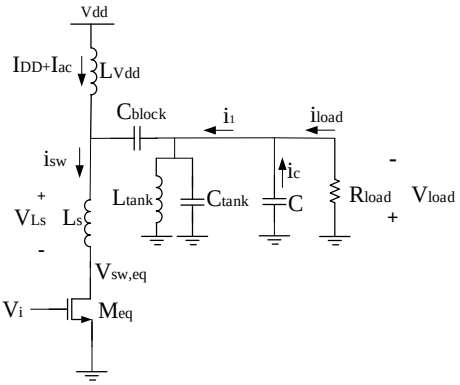

Figure 5. Equivalent half circuit for inverse E power amplifier

In the ON state, the switch current flows through inductor Ls. Therefore, using Equations (8) and (9), the equation describing the switch current in the ON state can be found as Equation (10).

$$i_{sw} = \frac{1}{\omega Ls}\int_0^{\theta}\left(V_{DD}\left(1-a\sin(\theta+\varphi)\right)-R_{sw,eq}i_{sw}\right)d\theta \quad (10)$$

As mentioned before, the following assumptions are made for switch current in transition from ON to OFF state.

$$i_{sw}\big|_{\theta=\pi} = i_0 \quad (11)$$

$$\left.\frac{di_{sw}}{d\theta}\right|_{\theta=\pi} = s_0 \quad (12)$$

By using Equation (11) we could solve Equation (10) to reach Equation (13).

$$i_{sw} = \begin{cases} i_{fad}+i_{cnst} & 0<\theta<\pi \\ 0 & \pi<\theta<2\pi \end{cases} \quad (13)$$

where, i_{fad} and i_{cnst} is defined as Equations (14) and (15).

$$i_{fad} = \left(i_0 - V_{DD}\frac{L_s{}^2\omega^2 + R_{sw}a\left(-\omega L_s\cos(\varphi)+R_{sw}\sin(\varphi)\right)}{R_{sw}\omega^2 L_s{}^2}\right)e^{\frac{-R_{sw}(\theta-\pi)}{\omega L_s}} \quad (14)$$

$$i_{cnst} = \frac{V_{DD}\left[L_s{}^2\omega^2 + R_{sw}a\left(\omega L_s\cos(\theta+\varphi)-R_{sw}\sin(\theta+\varphi)\right)\right]}{R_{sw}\omega^2 L_s{}^2} \quad (15)$$

The values of V_{DD} and ω depend on the technological constraints and the operating frequency of the transmitter respectivley. Therefore, by choosing the values of i_0, R_{sw} and s_0 as the design parameters, the values of a, L_s and φ should be determined.

The first equation to determine a, L_s and φ is achieved by replacing Equation (13) into Equation (12) which leads to Equation (16).

$$V_{DD}\left(1+a\sin\varphi\right) = R_{sw}i_0 + \omega L_s s_0 \quad (16)$$

The switch is OFF for π<θ<2π, so in the start of the next period (θ=0) the switch current should be equal to zero. Applying this fact to Equation (13) would lead us to Equation (17).

$$L_s\omega\cos\varphi - R_{sw}\sin\varphi = \frac{-\left(e^{\frac{R_{sw}\pi}{\omega L_s}}\left(R_{sw}i_0 - V_{DD}\right)+V_{DD}\right)\left(L_s{}^2\omega^2 + R_{sw}{}^2\right)}{aR_{sw}V_{DD}\left(e^{\frac{R_{sw}\pi}{\omega L_s}}+1\right)} \quad (17)$$

The power dissipated in R_{sw} when the switch is ON can be derived as Equation (18).

$$P_{Loss,switch} = \frac{1}{2\pi}\int_0^{2\pi} R_{sw}i_{sw}^2\,d\theta \quad (18)$$

The power stored in the switch shunt capacitance in the transition from OFF to ON state is dissipated as well as the energy stored in L_s in the trasnsition from ON to OFF. The sum of these two terms is called $P_{Loss,LC}$ and can be found as Equation (19).

$$P_{Loss,LC} = \frac{1}{2}\left(C_{sw}V_{sw0}^2 + L_s i_0^2\right)f \quad (19)$$

where, V_{sw0} is the switch voltage for θ=π and C_{sw} is the switch shunt capacitance.

Therefore, the total input power (P_{DC}) is the sum of the dissipated power in R_{sw}, L_s, C_{out} and the output power and can be expressed as Equation (20).

$$P_{DC} = P_{out} + \frac{1}{2}\left(C_{sw}V_{sw0}^2 + L_s i_0^2\right)f + \frac{1}{2\pi}\int_0^{2\pi} R_{sw}i_{sw}^2 d\theta \quad (20)$$

On the other hand P_{DC} can be expressed as Equation (21).

$$P_{DC} = \frac{V_{DD}}{2\pi}\int_0^{2\pi} i_{sw}\,d\theta \quad (21)$$

By combining Equations (20) and (21) the third equation to determine the parameters a, L_s and φ can be derived as Equation (22).

$$\frac{1}{2\pi}\int_0^{2\pi}\left(V_{DD}i_{sw} - R_{sw}i_{sw}^2\right)d\theta = P_{out} + \frac{1}{2}\left(C_{sw}V_{sw0}^2 + L_s i_0^2\right)f \quad (22)$$

So by using Equations (16), (17) and (22) the parameters a, L_s and φ can be found.

On the other hand, since V_{Lvdd}=Vo=V_c the following equations can be written considering Equation (8).

$$I_{L_{Vdd}} = \frac{V_{DD}a}{\omega L_{Vdd}}\left(\cos\varphi - \cos\left(\theta+\varphi\right)\right) \quad (23)$$

$$I_C = CV_{DD}a\omega\cos\left(\theta+\varphi\right) \quad (24)$$

In addition, by writing the switch current fourier series where its DC term would only pass the L_{Vdd} because of C_{block} and all harmonics except the fundamental one is absorbed by LC tank, we have Equations (25)-(27).

$$L_{Vdd} = \frac{V_{DD}a\cos\varphi}{\omega I_{DD}} \quad (25)$$

$$R_{Load} = \frac{aV_{DD}}{b_1} \quad (26)$$

$$C = \frac{a_1}{V_{DD}a\omega} + \frac{1}{\omega^2 L_{Vdd}} \quad (27)$$

where, a_1 and b_1 can be found by Equations (28) and (29) respectively.

$$a_1 = \frac{1}{\pi}\int_0^{2\pi} i_{sw}(\theta,\varphi)\cos\left(\theta+\varphi\right)d\theta \quad (28)$$

$$b_1 = \frac{1}{\pi}\int_0^{2\pi} i_{sw}(\theta,\varphi)\sin(\theta+\varphi)d\theta \quad (29)$$

Finally, the values of L_{tank} and C_{tank} depend on the tank's quality factor and can be found as Equations (30) and (31).

$$C_{tank} = \frac{Q_{LC}}{R_{Load}\omega} \quad (30)$$

$$L_{tank} = \frac{1}{\omega^2 C_{tank}} \quad (31)$$

By using the mentioned equations the inverse E power amplifer is designed for different values of i_0 and s_0. First the value of i_0 is kept equal to zero and the efficiency is found for different values of s_0. Then the s_0 corresponding to the best efficiency is chosen and the same process for finding i_0 which corresponds to the best efficiency is repeated with the previous stage s_0. Figure 6 shows the theoretical and simulation results for efficiency versus s_0 while i_0=0.

The power supply votage is equal to 1.8V while the switches aspect ratios are W/L=360µ/0.18µ. the output power and frequency are equal to 1W and 2.44 GHz as mentioned before.

As it can be seen the efficiency is not at its highest when s_0 is equal to zero. This is because in this work we considered the switch nonidealities therefore the ZCS and the ZCDS conditions for the best efficiency are not true. As it can be seen in Figure 6 the best efficiency occurs for s_0=-50mA/t so the efficiency is extracted for different values of i_0 while s_0 is equal to -50mA/t in Figure 7.

Figure 7 shows that the best efficiency occurs for i_0=300mA and s_0=-50mA/t. So the traditional ZCS and ZCDS conditions for the best efficiency in presence of the switch nonidealities are not true. Table 4 lists the circuit elements values for i_0=300mA and s_0=-50mA/t.

To ensure the circuit reliability the normalized voltages of the switches (according to Figure 4) is shown in Figure 8. As it can be seen the voltages do not reach $2V_{dd}$ which will prevent the circuit failure.

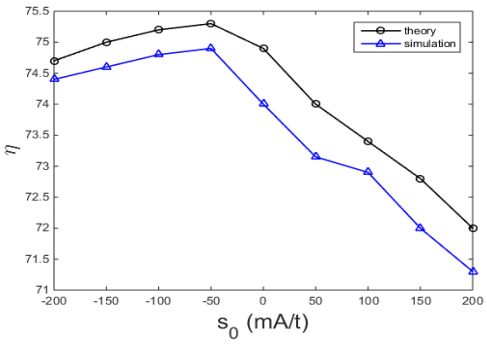

Figure 6. Efficiency versus s_0 while i_0=0

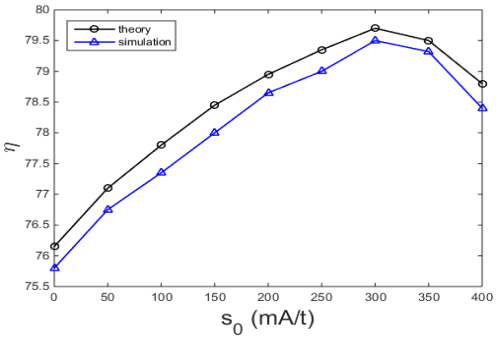

Figure 7. Efficiency versus i_0 while s_0=-50mA/t

TABLE 4. Circuit elements for E inverse PA

Ls (pH)	L_{vdd}(pH)	R_{load} (Ω)	C(pF)	L_{tank}(pH)	C_{tank}(pF)
152	474	10.8	17.2	88	48

The PA output versus its differential input power is shown in Figure 9. As it can be seen the $P_{in\text{-}1dB}$ is equal to 6.4 dBm while for having 30 dBm (1 watt) output the PA input power should be equal to 13 dBm. This means that the PA gain compression would increase the output EVM but because of the light modulation scheme and the data only being in the transmitted signal's phase, the linearity requirements of the transmitter is relaxed and the EVM would not be compromised heavily. This will be shown later in section 6.

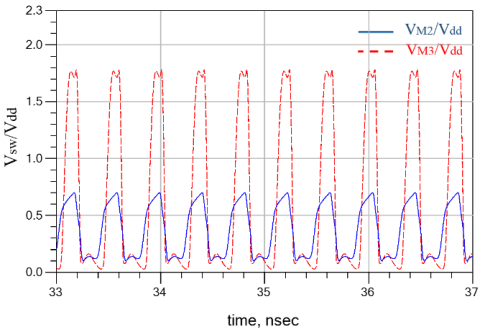

Figure 8. Normalized switch voltages

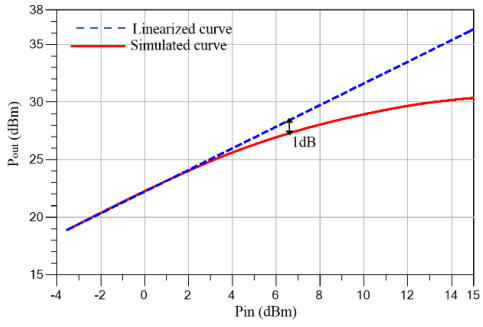

Figure 9. The PA output power versus its differential input power

4. UPCONVERTER DESIGN

Figure 10 depicts the upconverter used in this work. Here, a double balanced passive differential mixer is used. To reduce the baseband signal bandwidth to 80 MHz a LPF filter implemented in the baseband processor is used which consists of a raised cosine filter with rolloff factor α=0.35. Figure 11 shows the time and frequency responses of the filter and Figure 12 depicts the input and output signal of the filter.

To sum I and Q parts, the Gm network consisting of M_{12}-M_{15} is used. The tail current Im alongside the bias circuit (the dashed boxes) provide the needed bias for Gm networks while C_{cp} desensitize the bias point of the Gm networks from the output common mode level of the mixer and the C_{bp} provides the swing headroom needed for output voltage. The Gm network is also in charge of providing the necessary gain needed for the mixer signals to drive the PA therefore plays the part of preamplifier. The Lm-Cm tank alongside PA's input capacitance provides the bandpass filter to select the 80 MHz desired bandwidth. Also the differential architecture improves the linearity of the mixer which in turn enhances the EVM.

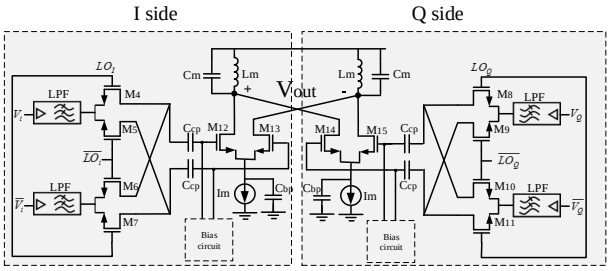

Figure 10. the upconverter

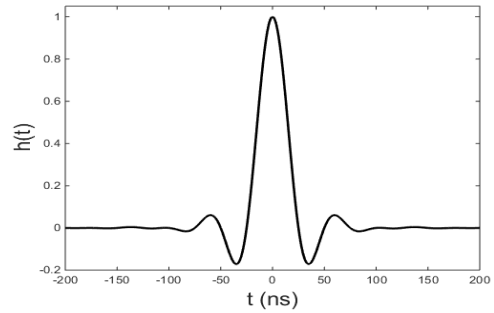

(a)

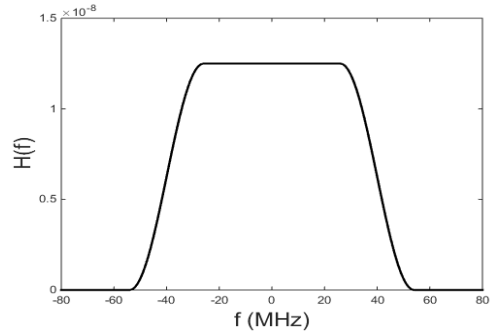

(b)

Figure 11. The raised cosine filter (a) time domain (b) frequency domain response

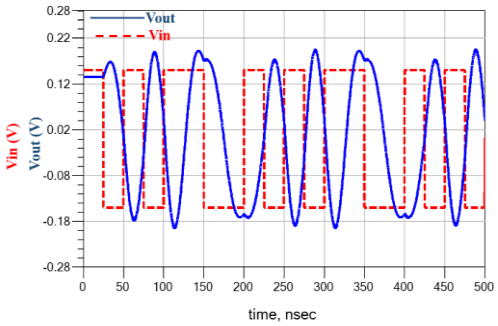

Figure 12. The raised cosine filter input and output

The mixer gain can be found as (32) and circuit elements values are listed in Table 5.

$$A_{mixer} = \frac{2\sqrt{2}}{\pi} g_{m12-15} R_{P_{Lm-Cm}} \quad (32)$$

where $gm_{12\text{-}15}$ is the M12-M15 transconductance, $Rp_{Lm\text{-}Cm}$ is the equivalent parallell resistance of the Lm-Cm resonator.

As it can be seen from Figure 13, the 1-dB compression point output power is equal to 16 dBm while from Figure 9 the mixer output power should be equal to 14 dBm for having 30 dBm PA output power. Therefore, the needed mixer output power is 2 dB lower than the 1-dB compression point and so it doesn not have significant effect on transmitter's EVM.

TABLE 5. Circuit elements for mixer

W/L ($M_{4\text{-}11}$)	W/L ($M_{12\text{-}15}$)	C_{bp} (pF)	C_{cp} (pF)	C_m (pF)	L_m (nH)	Im (mA)
36µ/0.18µ	54µ/0.18 µ	10	10	3.95	1.06	5

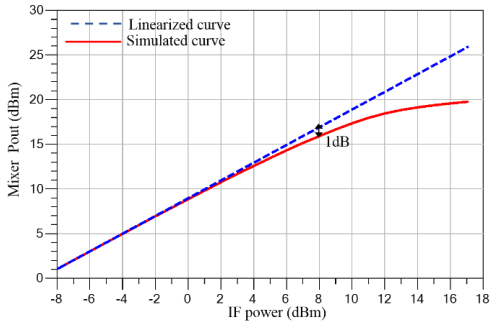

Figure 13. Mixer output power versus input IF power

Figure 14 shows that the mixer conversion gain for 6 dB IF input power which results in 14 dB needed power for PA input is equal to 8.3 dB. The IF input power is provided by the baseband processor.

5. QUADRATURE OSCILLATOR DESIGN

The oscillator is responsible for providing the carrier signal. The I/Q mismatches could cause in phase and amplitude errors which in turn deviate the signal constellation from its ideal values and increase the EVM [6]. Studies show that mismatches among the LC tank elements are the main source of phase and amplitude errors [27, 28]. So to overcome this issue, we used the structure proposed in [29] which is shown in Figure 15.

It is shown in [29] that by choosing $K_1=1/K_2$ the phase and amplitude errors could decrease and even reach zero. To achieve this, the tune circuit (confined in grey box) is used. The constant I_{tune} is divided between M13 and M14 according to $\Delta V_{tune}=V_{tune1}-V_{tune2}$. So by increasing V_{tune1} , M11 drain current decreases while increasing current flowing through M12. The currents of M11 and M12 are mirrored to M9 and M10 respectively providing I_{cp1} and I_{cp2}. It can be seen that for little values of ΔV_{tune}, K_1 woud be equal to $1/K_2$ fulfilling the conditions for zeroing phase and amplitude errors [29]. To test this, mismatches between tank's inductor and capacitor is applied to the circuit ranging from 1 to 5% and the phase and amplitude errors with $K_1=K_2$ (without calibration) and $K_1=1/K_2$ (with calibration) is extracted and shown in Figure 16.

As it can be seen the phase and amplitude errors are cancelled by using the calibration method. To ensure that calibration would not impose excessive phase noise to circuit outputs, the circuit phase noise before and after calibration at 1 MHz offset is shown in Figure 17.

Figure 17 shows that calibration does not have any undesirable effect on the phase noise and therefore EVM would not deteriorate by using this technique.

6. TRANSMITTER CHARACTERISTICS

Figure 18 shows the shaped single ended I signal and the corresponding downconveted signal from PA output. As it can be seen the downconverted signal is quite the same as the shaped signal. To determine the quality of the transmitted signal, the EVM is measured and the corresponding constellation is depicted in Figure 19. Figure 19 shows that inspite of the PA compression, because of the light modulation scheme the signals are quite distinguishable.

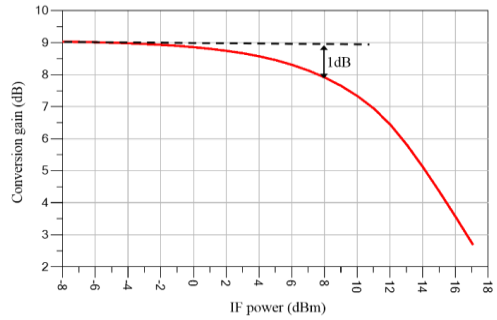

Figure 14. Mixer conversion gain versus input IF power

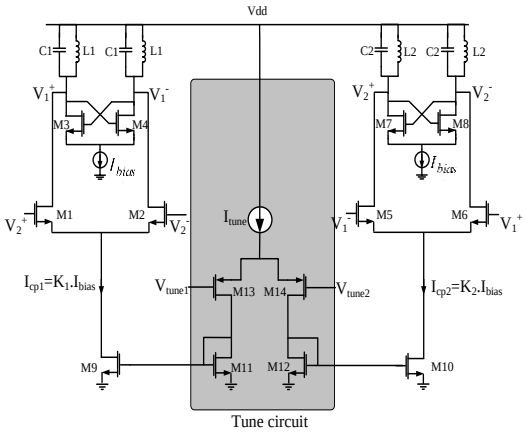

Figure 15. Tunable quadratue LC oscillator

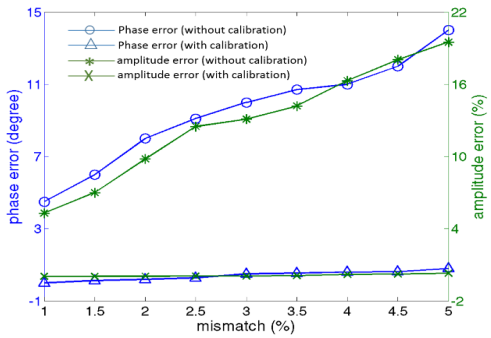

Figure 16. Quadratue LC oscillator phase and amplitude errors versus mismatches

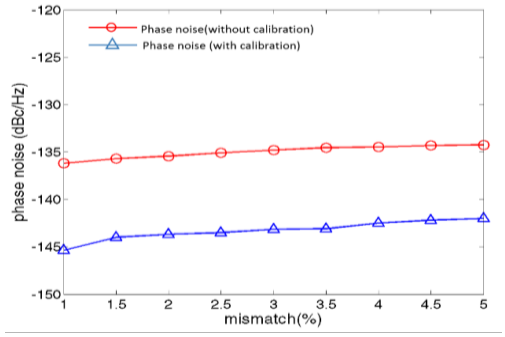

Figure 17. Quadratue LC oscillator phase noise with and without calibration at 1MHz offset

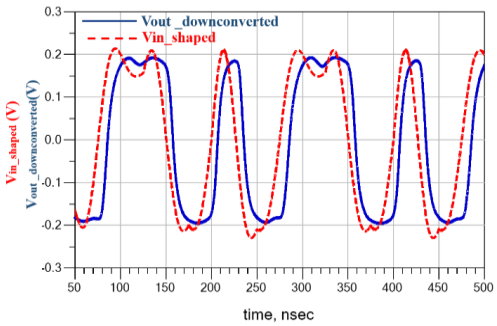

Figure 18. The shaped single ended I signal and the corresponding downconveted I signal

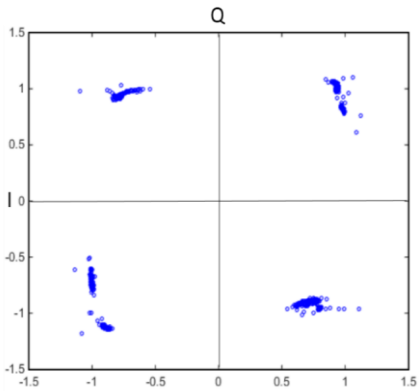

Figure 19. The signal output constellation

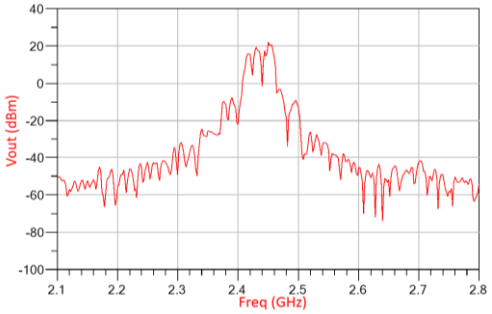

Figure 20. The signal output spectrum

The transmitter output spectrum is shown in Figure 20. The power consumption of power amplifier is equal to 1.3W while the quadrature oscillator and mixer alongside preamplifier only consume 41 and 18 mW respectively. The transmitter characteristics are listed and compared with other works in Table 6.

As it can be seen in Table 6, our work has the best efficiency. This is because firstly we choose a light modulation scheme which allows us to utilize a nonlinear PA and secondly we optimize the PA considering the switch nonidealities. Although the EVM for our work is higher than others but the light modulation relaxes the EVM requirements for signal recovery.

TABLE 6. Transmitter characteristics comparison with other works

	Supply Voltage (V)	Architecture	Center Frequency (GHz)	Technology	Output power (dBm)	Transmitter efficiency (%)	EVM (dB)	ACPR (dBc)
This work	1.8	Direct conversion	2.4	0.18 µ CMOS	30	73.4	-16	-32.75
[30]	2	Direct conversion	2.6	0.18 µ CMOS	15	23 (PA only)	-30.45	-43
[31]	3.3	Modern direct conversion	2.4	0.18 µ CMOS	17.3	7.3	-28.1	-35
[32]	2.05	Direct conversion (outphasing)	2.4	32nm CMOS	20	18.6	-25	-45
[33]	1.8	Direct conversion	2.4	40nm CMOS	18.8	15	-25	-40

7. CONCLUSION

In this work we designed a high efficiency, high range spread spectrum transmitter. By choosing a high process gain in the system level design we showed that the transmitter could reach a range of 55 Km while consuming 1.359 W. Because of using light modulation scheme we could employ an inverse class E nonlinear power amplifier which improves the transmitter efficiency significantly while our design takes PA's switching nonidealities into account to find the best conditions for efficiency. The double balanced passive mixer used in this work does not share into the transmitter compression while by choosing tunable quadrature oscillator we could cancel the phase and amplitude errors without compromising the phase noise. The EVM extracted for this work is equal to -32.75 dBc which is high enough to detect the received signal because of using QPSK modulation.

8. REFERENCES

1. Goldsmith, A., Wireless communications. Cambridge university press., (2005).
2. Tse, D. and Viswanath, P., Fundamentals of wireless communication, Cambridge university press, (2005).

3. Crilly, P.B., Communication systems: An introduction to signals and noise in electrical communication, McGraw-Hill Companies, Inc., (2010).
4. Rofougaran, A., Chang, G., Rael, J.J., Chang, J.C., Rofougaran, M., Chang, P.J., Djafari, M., Ku, M.K., Roth, E.W., Abidi, A.A. and Samueli, H., "A single-chip 900-MHz spread-spectrum wireless transceiver in 1-μm CMOS. I. Architecture and transmitter design," ***IEEE Journal of Solid-State Circuits***, Vol. 33, No. 4, (1998), 515–534.
5. Peterson, R., Ziemer, R., and Borth, D., Introduction to spread-spectrum communications, (Vol. 995), New Jersey: Prentice hall, (1995).
6. Razavi, B. and Behzad, R., RF microelectronics, (Vol. 1), New Jersey: Prentice hall, (1998).
7. Lee, K.Y., Lee, S.W., Koo, Y., Huh, H.K., Nam, H.Y., Lee, J.W., Park, J., Lee, K., Jeong, D.K. and Kim, W., "Full-CMOS 2-GHz WCDMA direct conversion transmitter and receiver," ***IEEE Journal of Solid-State Circuits***, Vol. 38, No. 1, (2003), 43–53.
8. Choi, C., Choi, J., Kim, M., Park, H. and Nam, I., "A low power 2.4-GHz CMOS direct-conversion transmitter for IEEE 802.15.4," In IEEE International Wireless Symposium (IWS 2014), IEEE, (2014), 1–4.
9. Mazzanti, A., Svelto, F., and Andreani, P., "On the Amplitude and Phase Errors of Quadrature LC-Tank CMOS Oscillators," ***IEEE Journal of Solid-State Circuits***, Vol. 41, No. 6, (2006), 1305–1313.
10. GHonoodi, H. and Miar Naimi, H., "Canceling tradeoff between phase noise and phase error in parallel coupled quadrature oscillators," In 18th Iranian Conference on Electrical Engineering, IEEE, (2010), 459–464.
11. Hsiao, C.H., Li, C.J., Wang, F.K., Horng, T.S. and Peng, K. C., "Analysis and Improvement of Direct-Conversion Transmitter Pulling Effects in Constant Envelope Modulation Systems," ***IEEE Transactions on Microwave Theory and Techniques***, Vol. 58, No. 12, (2010), 4137–4146.
12. Hsiao, C.H., Chen, C.T., Horng, T.S. and Peng, K. C., "Direct-conversion transmitter with resistance to local oscillator pulling in non-constant envelope modulation systems," In IEEE MTT-S International Microwave Symposium, (2011), 1–4.
13. Krivokapic, I. and Oskovsky, M., "GTEM cell method based comparative analysis of performance degradation in integer and fractional frequency synthesizer based direct conversion CDMA transmitters," In Proceedings of the 2005 IEEE International Frequency Control Symposium and Exposition, IEEE, (2005), 569–574.
14. Ting-Ping Liu, "A 2.7-V dual-frequency single-sideband mixer [for PCS]," In Symposium on VLSI Circuits. Digest of Technical Papers (Cat. No.98CH36215), IEEE, (1998), 124–127.
15. Hanif, M.F., Askari, S., Desai, K., Banerjee, B. and Nourani, M., "A direct conversion WiMAX RF transmitter in 0.18um CMOS technology," In IEEE Dallas Circuits and Systems Workshop (DCAS), IEEE, (2009), 1–4.
16. Abu-Rgheff, M.A., Introduction to CDMA Wireless Communications, Academic Press, Inc. Orlando, FL, USA, (2007).
17. Ziemer, R.E. and Peterson, R.L., Introduction to digital communication, New York: Maxwell Macmillan, (1992).
18. Proakis, J. and Salehi, M., Digital communications, New York: McGraw-hill, (2007).
19. El-Hamamsy, S.A., "Design of high-efficiency RF Class-D power amplifier," ***IEEE Transactions on Power Electronics***, Vol. 9, No. 3, (1994), 297–308.
20. El-Desouki, M.M., Deen, M.J. and Haddara, Y.M., "A low-power CMOS class-E power amplifier for biotelemetry applications," In 2005 European Microwave Conference, IEEE, (2005), 1–4.
21. Kim, J.Y., Chun, S.H., Jang, D.H., Kim, J.H. and Kennedy, G. P., "A 1-kW switchable damped class-E power amplifier for plasma processing applications," ***Microwave and Optical Technology Letters***, Vol. 52, No. 11, (2010), 2438–2441.
22. Eroglu, A. and Sivakumar, S., "Phase controlled Class E amplifiers for pulsing applications," In IEEE MTT-S International Microwave Symposium Digest, IEEE, (2009), 765–768.
23. Sokal, N. O. and Sokal, A. D., "Class E-A new class of high-efficiency tuned single-ended switching power amplifiers," ***IEEE Journal of Solid-State Circuits***, Vol. 10, No. 3, (1975), 168–176.
24. Lee, Y.S., Lee, M.W., Kam, S.H. and Jeong, Y. H., "A High-Efficiency GaN-Based Power Amplifier Employing Inverse Class-E Topology," ***IEEE Microwave and Wireless Components Letters***, Vol. 19, No. 9, (2009), 593–595.
25. Typpo, J., Hietakangas, S., and Rahkonen, T., "A 900 MHz 10 mW monolithically integrated inverse class E power amplifier," In NORCHIP 2010, IEEE, (2010), 1–4.
26. Chen, P. and He, S., "Investigation of Inverse Class-E Power Amplifier at Sub-Nominal Condition for Any Duty Ratio," ***IEEE Transactions on Circuits and Systems I: Regular Papers***, Vol. 62, No. 4, (2015), 1015–1024.
27. Romanò, L., Levantino, S., Samori, C. and Lacaita, A. L., "Multiphase LC oscillators," ***IEEE Transactions on Circuits and Systems I: Regular Papers***, Vol. 53, No. 7, (2006), 1579–1588.
28. Seifi, S. and H.Miar-Naimi, "Analysis of Oscillation Amplitude and Phase Error in Multiphase LC Oscillators," ***International Journal of Engineering - Transactions C: Aspects***, Vol. 26, No. 6, (2013), 587–596.
29. GHonoodi, H. and Naimi, H.M., "A Phase and Amplitude Tunable Quadrature LC Oscillator: Analysis and Design," ***IEEE Transactions on Circuits and Systems I: Regular Papers***, Vol. 58, No. 4, (2011), 677–689.
30. Hanif, M.F., Askari, S., Desai, K., Banerjee, B. and Nourani, M., "A direct conversion WiMAX RF transmitter in 0.18um CMOS technology," In IEEE Dallas Circuits and Systems Workshop (DCAS), IEEE, (2009), 1–4.
31. Wang, P.C., Chang, C.J., Chiu, W.M., Chiu, P.J., Wang, C.C., Lu, C.H., Chen, K.T., Huang, M.C., Chang, Y.M., Lin, S.M. and Chan, K.U., "A 2.4GHz Fully Integrated Transmitter Front End with +26.5-dBm On-Chip CMOS Power Amplifier," In IEEE Radio Frequency Integrated Circuits (RFIC) Symposium, IEEE, (2007), 263–266.
32. Madoglio, P., Ravi, A., Xu, H., Chandrashekar, K., Verhelst, M., Pellerano, S., Cuellar, L., Aguirre, M., Sajadieh, M., Degani, O. and Lakdawala, H., "A 20dBm 2.4GHz digital outphasing transmitter for WLAN application in 32nm CMOS," In IEEE International Solid-State Circuits Conference, IEEE, (2012), 168–170.
33. Lu, C., Wang, H., Peng, C.H., Goel, A., Son, S., Liang, P., Niknejad, A., Hwang, H.C. and Chien, G., "A 24.7dBm all-digital RF transmitter for multimode broadband applications in 40nm CMOS," In IEEE International Solid-State Circuits Conference Digest of Technical Papers, IEEE, (2013), 332–333.

Design of a High Range, High Efficiency Spread Spectrum Transmitter for Audio Communication Applications

S. Seifi, H. Miar Naimi, S. M. H. Andargoli

Department of Electrical Engineering, Babol University of Technology, Babol, Iran

P A P E R I N F O

Paper history:
Received 05 November 2018
Received in revised form 23 April 2019
Accepted 02 May 2019

Keywords:
Direct Sequence Spread Spectrum
Double Balanced Passive Mixer
Error Vector Magnitude
Inverse E Power Amplifier
Switching Power Amplifier
Tunable Quadrature Oscillator
Wireless Transmitter

چکیده

این کار یک فرستنده‌ی طیف گسترده‌ی توالی مستقیم با برد و بازده بالا برای برقراری یک ارتباط صوتی را پیشنهاد می‌دهد. نشان داده شده است که با انتخاب بهره‌ی پردازش بالا سیگنال داده می‌تواند به بردی برابر با ۵۵ کیلومتر در باند ISM ۲/٤ GHz برسد. با انتخاب یک مدولاسیون سبک، شرایط SNR و در نتیجه EVM مورد نیاز برای داشتن نرخ خطای بیت کم ساده‌تر می‌شود. بنابراین در این کار از یک تقویت‌کننده توان سوییچینگ استفاده شده که باعث افزایش بازده فرستنده شده و علاوه بر آن اثرات سوییچ غیر ایده‌آل در تقویت‌کننده‌ی توان در نظر گرفته شده و معادلات مورد نیاز برای استخراج شرایط جدید در مقایسه با شرایط مرسوم سوییچینگ جریان و مشتق جریان صفر استخراج شده است. بازده و توان خروجی تقویت‌کننده به ترتیب ۷۹/۵٪ و ۳۰ dBm می‌باشد. میکسر و پیش تقویت‌کننده‌ی توان بهره تبدیلی برابر با ۹ dB و نقطه‌ی فشردگی ۱ dB خروجی برابر با ۱٦ dBm دارند و نوسان‌ساز متعامد قابل تنظیم استفاده شده توانایی حذف خطای دامنه و فاز را بدون خراب کردن نویز فاز را دارد. فرستنده دارای بازده ۷۳/٤٪ با EVM برابر ۳۲/۷۵ dB– می‌باشد.

***doi**: 10.5829/ije.2019.32.08b.10*